Article

Current Biology

Transient Tissue-Scale Deformation Coordinates Alignment of Planar Cell Polarity Junctions in the Mammalian Skin

Highlights

- Axial PCP asymmetry arises with tissue-scale deformation and cell rearrangements
- Reorienting tissue deformation is sufficient to alter the Celsr1 polarity axis
- Local PCP arises spontaneously in vitro and reorients upon cell rearrangements
- The PCP axis aligns with persistent cell interfaces during neighbor exchanges

Authors

Wen Yih Aw, Bryan W. Heck, Bradley Joyce, Danelle Devenport

Correspondence

danelle@princeton.edu

In Brief

The global cues that function to initiate and coordinate planar cell polarity (PCP) asymmetry in mammalian tissues remain unknown. Aw et al. show that axial PCP alignment in the skin epidermis evolves concomitantly with transient tissue strain and Celsr1 asymmetry emerges upon force-induced remodeling of intercellular junctions.

Aw et al., 2016, Current Biology *26*, 2090–2100
August 22, 2016
http://dx.doi.org/10.1016/j.cub.2016.06.030

CellPress

CellPress

Current Biology
Article

Transient Tissue-Scale Deformation Coordinates Alignment of Planar Cell Polarity Junctions in the Mammalian Skin

Wen Yih Aw,[1] Bryan W. Heck,[1] Bradley Joyce,[1] and Danelle Devenport[1,*]
[1]Department of Molecular Biology, Princeton University, Princeton, NJ 08544, USA
*Correspondence: danelle@princeton.edu
http://dx.doi.org/10.1016/j.cub.2016.06.030

SUMMARY

Planar cell polarity (PCP) refers to the collective alignment of polarity along the tissue plane. In skin, the largest mammalian organ, PCP aligns over extremely long distances, but the global cues that orient tissue polarity are unknown. Here, we show that Celsr1 asymmetry arises concomitant with a gradient of tissue deformation oriented along the medial-lateral axis. This uniaxial tissue tension, whose origin remains unknown, transiently transforms basal epithelial cells from initially isotropic and disordered states into highly elongated and aligned morphologies. Reorienting tissue deformation is sufficient to shift the global axis of polarity, suggesting that uniaxial tissue strain can act as a long-range polarizing cue. Observations both in vivo and in vitro suggest that the effect of tissue anisotropy on Celsr1 polarity is not a direct consequence of cell shape but rather reflects the restructuring of cell-cell interfaces during oriented cell divisions and cell rearrangements that serve to relax tissue strain. We demonstrate that cell intercalations remodel intercellular junctions predominantly between the mediolateral interfaces of neighboring cells. This restructuring of the cell surface polarizes Celsr1, which is slow to accumulate at nascent junctions yet stably associates with persistent junctions. We propose that tissue anisotropy globally aligns Celsr1 polarity by creating a directional bias in the formation of new cell interfaces while simultaneously aligning the persistent interfaces at which Celsr1 prefers to accumulate.

INTRODUCTION

The collective polarization of cellular structures, such as cilia, hairs, and feathers, is a widely conserved attribute of epithelial tissues termed planar cell polarity (PCP). During the development of PCP, cells integrate global directional cues with local cell-to-cell communication to form precise and collectively aligned patterns that extend over extremely long distances [1–4]. Fundamental to the establishment of planar polarity is asymmetric positioning of a set of "core PCP proteins," whose polarized distributions can be classified as either *axial* or *vectorial*. Flamingo (Fmi) (Celsr in vertebrates), an atypical cadherin, displays axial asymmetry, where it forms homodimers across junctions oriented along one tissue axis but is excluded from orthogonal junctions [5–8]. In contrast, Frizzled (Fz) and Van Gogh (Vang) display vectorial asymmetry, where they are recruited to Fmi/Celsr1 junctions at opposite poles of the cell [9, 10]. Tissue-level directional cues must bias both the PCP axis and the PCP vector, but the global cues that orient either of these asymmetries remain poorly understood.

Current insights from *Drosophila* regarding the global cues proposed to bias PCP localization generally fall into two classes: concentration gradients and physical forces. Concentration gradients are thought to orient vectorial asymmetry by biasing Fz accumulation toward one side of the cell [11]. In one model, opposing gradients of Dachsous and Four-jointed promote PCP asymmetry by biasing the direction of Fz transport [12–14]. In another model, a Wnt concentration gradient orients the PCP vector by creating cellular gradients of Fz activity [15–18]. Mechanical cues, by contrast, predominantly affect axial asymmetry. For example, during *Drosophila* pupal wing morphogenesis, anisotropic mechanical forces reshape the wing blade and, concomitantly, reorient PCP alignment from a radial to proximal-distal orientation—providing a new axis to the existing vectorial asymmetries [19]. Here, we focus on the latter phenomenon of axial PCP alignment by investigating the emergence of coordinated Celsr1 asymmetry over long distances in the mammalian skin.

PCP is responsible for the precise alignment of hair follicles across the murine epidermis [8, 20, 21]. These polarized multicellular units derive from embryonic basal cells, a single layer of progenitor cells whose polarization marks the first visible sign of PCP in the skin [8]. During embryogenesis, the core PCP proteins Celsr1, Vangl2, and Fz6 become asymmetrically localized in basal cells from initially disordered distributions. This redistribution establishes axial and vectorial asymmetry, where PCP proteins are enriched at anterior and/or posterior cell borders and depleted from medial-lateral borders [8, 22]. The PCP pattern in the basal layer prefigures the orientation of hair follicles, which grow with an anterior vector and align precisely along the anterior-posterior axis [8, 22].

Here, we demonstrate that Celsr1 asymmetry emerges temporally and spatially with a gradient of tissue deformation, which we propose acts as a long-range polarity cue. We find that Celsr1 localization becomes progressively biased toward

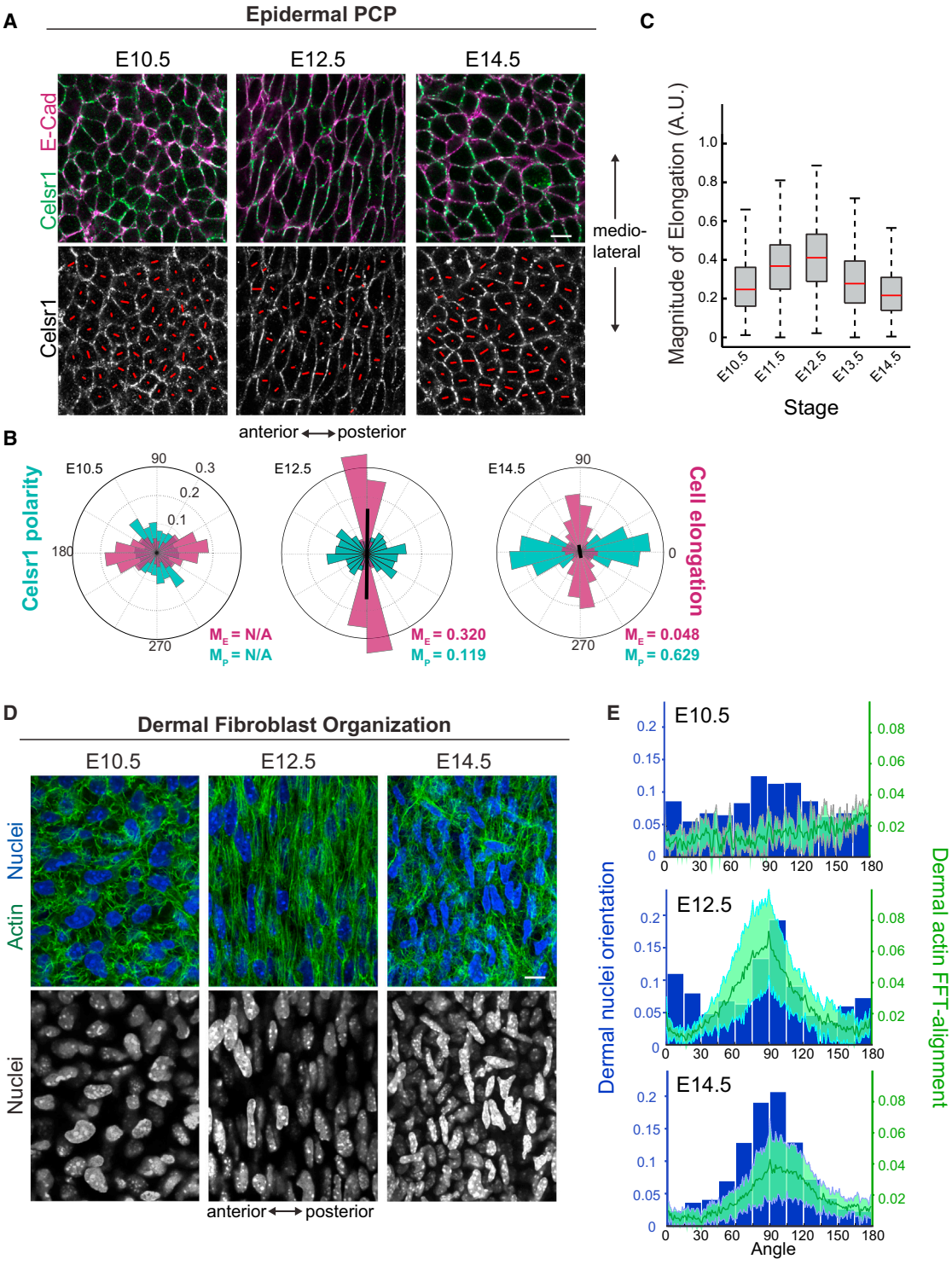

Figure 1. Temporal Evolution of Celsr1 Polarity

(A) Confocal planar sections through basal layer of whole-mount E10.5–E14.5 back skin labeled with Celsr1 (green) and E-cadherin (magenta). In all figures, anterior is left. Red lines within individual cells denote magnitude (length of line) and axis of Celsr1 polarity.

(B) Angular distribution of Celsr1 polarity and cell deformation from E10.5 to E14.5 back skin. E10.5, three embryos (871 cells); E12.5, eight embryos (614 cells); E14.5, 13 embryos (7,179 cells). M_P, magnitude of average polarity; M_E, magnitude of average cell elongation. The significance of the angular variation within each stage was assessed using a nonparametric permutation test. Statistical significance = $p < 0.05$ (if $p \geq 0.05$, M_P or M_E = N/A).

(C) Quantification of basal epidermal cell shape anisotropy from E10.5 to E14.5.

(D) Whole-mount immunofluorescence of E10.5, E12.5, and E14.5 back skins labeled for F-actin (green) and nuclei (Hoechst, blue) imaged in the dermis.

(legend continued on next page)

anterior-posterior cell interfaces as basal cells are transiently deformed and relaxed along the medial-lateral axis. Consistent with our hypothesis, externally applied uniaxial tension is sufficient to reorient the global axis of polarity. The effect of tissue deformation on Celsr1 polarity appears not to be a direct consequence of cell shape but rather reflects the oriented restructuring of cell-cell interfaces when cells rearrange, which likely functions to relieve anisotropic tissue strain. Using a spontaneously polarized organotypic culture system, we demonstrate that Celsr1 is slow to accumulate at newly formed junctions yet stably associates with persistent junctions. As a result, Celsr1 polarity emerges and shifts with the formation of new cell interfaces during neighbor exchange. We further demonstrate that junctionally localized Celsr1 has a lower turnover rate than E-cadherin, which helps to explain the coupling of Celsr1 polarization with new junction formation. Together, these results support a model where uniaxial tissue tension aligns Celsr1 polarity across the epidermis by creating a directional bias in tissue mechanics along one tissue axis.

RESULTS

The Establishment of PCP Asymmetry in the Murine Skin Correlates Temporally with Anisotropic Tissue Deformation

In several epithelial systems, the establishment of PCP asymmetry involves progressive redistribution of core PCP proteins from initially disordered states [8, 23, 24]. A challenge in relatively large tissues, such as the skin, is that PCP proteins must redistribute according to directional cues that bias asymmetry over very long distances. The long-range alignment of PCP could arise from local initiation and propagation [24] or via cues that act relatively synchronously across tissues. To determine whether PCP asymmetry arises in a spatiotemporal pattern across the skin, we performed a quantitative analysis of polarity establishment across large regions of the dorsal epidermis over time. PCP asymmetry was quantified by calculating nematic order of the integrated fluorescence intensity values of Celsr1 at cell borders beginning at embryonic day 10.5 (E10.5) [19]. This method detects subtle asymmetries in cortical localization, which were first apparent in basal cells at E11.5, 2 days earlier than we previously detected [8]. At this stage, Celsr1 accumulation was slightly biased to anterior and posterior cell borders. Over the next 3 days (E12.5– E14.5) this bias became progressively more pronounced as both the magnitude of Celsr1 polarity and its collective alignment increased (Figures 1A and 1B) [8].

We noted that the temporal progression of Celsr1 asymmetry in the epidermis correlated with striking and patterned changes in morphology. At the onset of Celsr1 polarization, basal cells collectively changed shape, becoming highly elongated along the medial-lateral axis and shortened along the anterior-posterior axis (Figures 1A–1C). Cell elongation peaked between days E11.5 and E12.5 and was followed by a phase of tissue relaxation at E13.5–E14.5, whereby basal cells returned to more isometric morphologies (Figures 1A–1C). Moreover, these cell shape changes were accompanied by cytoskeletal reorganization, where actin and microtubule filaments rearranged into highly aligned bundles oriented parallel to the cells' long axes (Figure S1). To understand the relationship between PCP asymmetry and epithelial morphology, we plotted Celsr1 polarity relative to cell elongation and found it was consistently oriented perpendicular to the axis of elongation (Figure 1B). E-cadherin localization, by contrast, was relatively uniform, irrespective of embryonic stage or cell shape (Figure S2), demonstrating that Celsr1 polarity measurements were not artifacts of changes in cell geometry.

Uniaxial tissue strain was also evident in the stroma that underlies the skin epithelium, as dermal fibroblasts reorganized with the same spatial and temporal dynamics as cell elongation in the basal layer. Whereas fibroblasts at E10.5 displayed roughly circular nuclei and randomly organized actin filaments, E12.5 fibroblasts were elongated and aligned along the medial-lateral axis (Figures 1D and 1E). Dermal fibroblast alignment persisted through E14.5 in interfollicular regions of the skin (Figures 1D and 1E), but deeper into the dermis, fibroblasts were less obviously organized (data not shown). These observations suggest that the entire outer skin surface is subject to tissue-scale deformations that correlate with the timing and direction of Celsr1 asymmetry.

Spatial Correlations between PCP Asymmetry and Epidermal Deformation

We hypothesized that the deformation of basal cells might serve as a global directional cue to orient Celsr1 polarity. If true, the correlation between tissue deformation and PCP asymmetry should also be observed in regions of the skin where polarity is known to reorient. For example, in dorsal skin, hair follicles align along the anterior-posterior axis, but in the limbs, they are shifted by 90 degrees to align with the proximal-distal axis. As expected, Celsr1 was enriched at proximal-distal cell borders in the limb, prefiguring the direction of hair follicle polarization (Figure 2A). Consistent with our observations at the dorsal skin surface, dermal fibroblast organization and basal cell elongation were shifted by 90° in this region, aligning circumferentially around the limb, and perpendicular to Celsr1 polarity axis (Figure 2A). These data demonstrate that there is close spatial correlation between epithelial elongation, dermal organization, and the orientation of Celsr1 polarity.

Interestingly, we observed patterned cell deformation and Celsr1 polarization along the dorsal back skin (Figures 2B and 2C). Basal cells located near the midline at E13.5 were highly elongated and displayed strong Celsr1 asymmetry, whereas cells located more laterally were more isotropic, weakly polarized, and poorly aligned (Figures 2B, 2C, and S3). The transition from strong to weak polarization was gradual along the medial-lateral

(E) 2D-fast Fourier transform was performed to measure the orientation of dermal actin fibers. Radial summation of pixel distribution was plotted between 0 and 180 degrees (anterior-posterior; mean ± SD). Note that location of the peak corresponds to principal orientation of fiber alignment and the peak height corresponds to overall fiber anisotropy; E10.5, four embryos (705 cells); E12.5, three embryos (401 cells); E14.5, 11 embryos (2,094 cells).
Scale bars represent 10 μm. See also Figures S1 and S2.

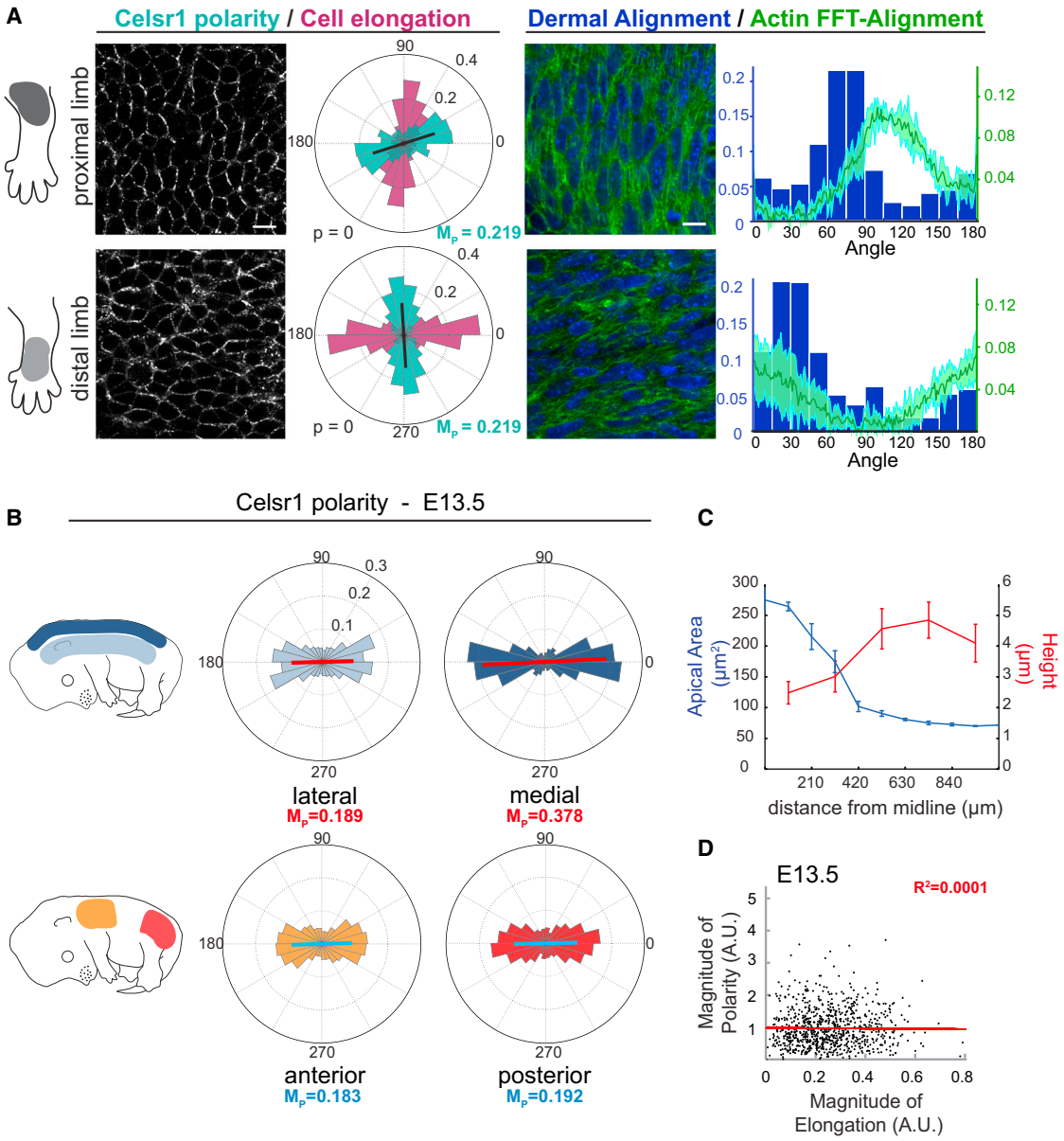

Figure 2. Spatial Correlation of Celsr1 Polarity with Tissue Anisotropies

(A) Confocal sections through epidermis and dermis of E14.5 proximal and distal forelimbs. Distribution plots show the orientation of Celsr1 polarity, basal cell elongation, dermal fibroblast orientation, and actin alignment. Note the reorientation of Celsr1 polarity and cell alignments from proximal to distal limb regions (n = 3 embryonic forelimbs).

(B) Distribution of Celsr1 polarity and cell elongation along mediolateral and anteroposterior axes of E13.5 back skins (n = 7). Note that the magnitude of average Celsr1 polarity (M_P) increases from lateral to medial.

(C) Quantified apical surface area and cell height along mediolateral axis. Cells along the midline are longer and flatter.

(D) Lack of correlation between magnitude of Celsr1 polarity and cell elongation on a cell-by-cell basis. n = 7 embryos (850 data points randomly selected from 5,702 cells).

Scale bars represent 10 μm. See also Figure S3.

axis such that cells at intermediate positions displayed intermediate elongation and Celsr1 asymmetry (Figure S3). By contrast, along the anterior-posterior axis, differences in Celsr1 asymmetry were not detected (Figure 2B). Thus, a tissue-level, medial-to-lateral gradient of cell deformation correlates with the direction and magnitude of epidermal planar polarity.

Reorienting the Direction of Tissue Strain Is Sufficient to Shift the PCP Axis

To test the hypothesis that uniaxial tissue deformation serves as a global cue to orient the axis of Celsr1 asymmetry, we designed a stretch chamber to culture skin explants on stretchable substrates (Figure 3G). Dorsal skin explants from E14.5 embryos

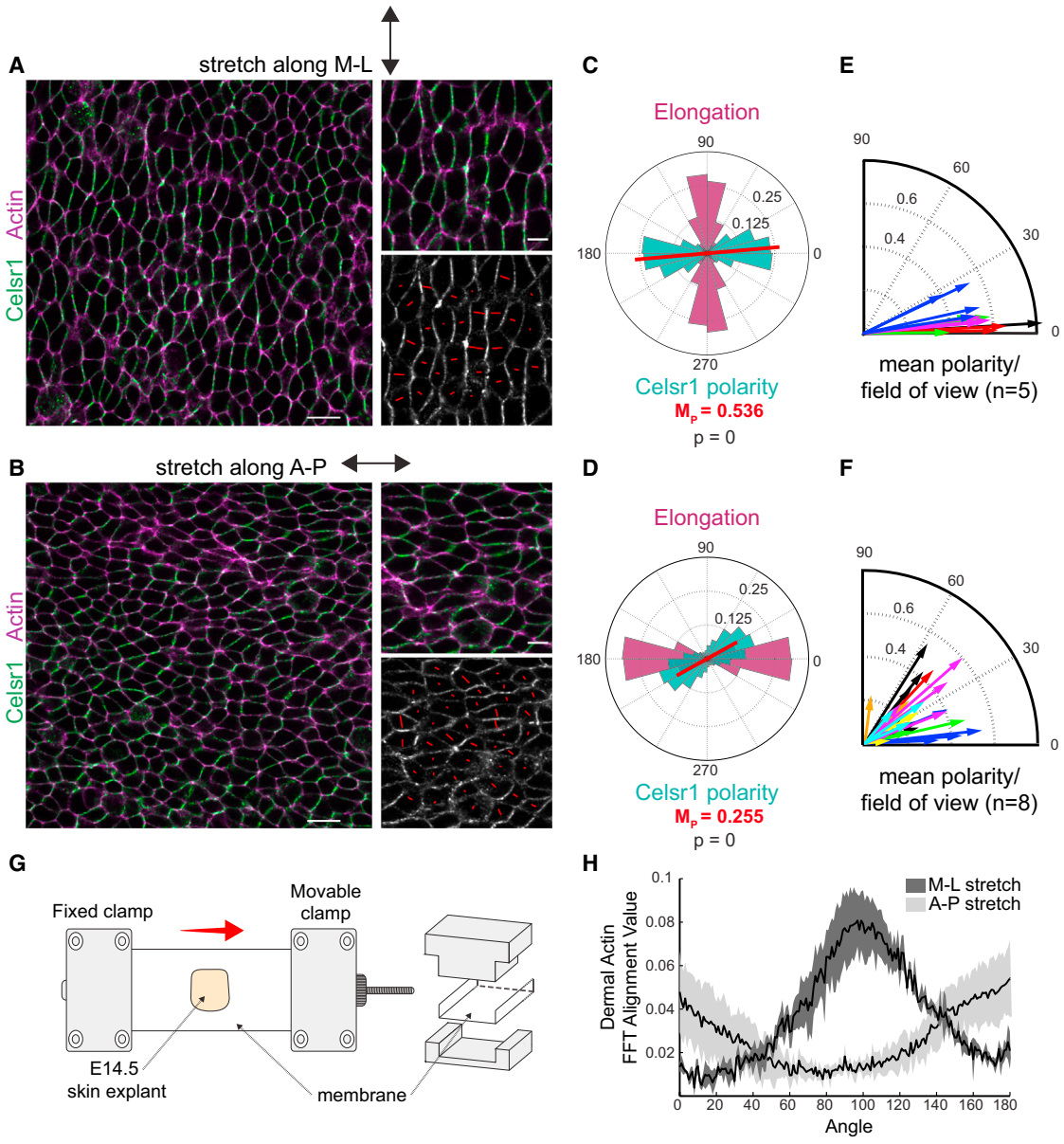

Figure 3. Celsr1 Polarity Reorients upon Exogenous Stretch

(A and B) Images of E14.5 back skins labeled for Celsr1 (green) and actin (magenta) captured 24 hr after stretching either along mediolateral or anterior-posterior axis.

(C and D) Distribution plots of basal cell elongation and Celsr1 polarity.

(E and F) Compass plots show the average orientation of Celsr1 polarity from individual fields of view. The length of each line defines average magnitude of polarity (per field of view). Paired samples are plotted in the same color.

(G) Experimental design for stretching explants.

(H) Quantification of dermal actin alignments in stretched E14.5 back skins (mean ± SD).

Scale bars represent 20 μm (A and B) and 10 μm (insets). See also Figure S4.

were attached to polydimethylsiloxane (PDMS) membranes, stretched in 1.0 mm steps every 30 min, and held at 25% displacement for 24 hr. When control explants were stretched along the normal (medial-lateral) axis, basal cells elongated mediolaterally in coordination with underlying dermal fibroblasts and Celsr1 displayed robust anterior-posterior polarization (Figures 3A, 3C, 3E, and 3H). By contrast, stretching skin explants perpendicular to the medial-lateral axis was sufficient to cause a 90-degree reorientation in basal cell elongation and dermal fibroblast alignment (Figures 3B, 3D, and 3H). Importantly, this mechanical perturbation was also sufficient to shift the global axis of PCP asymmetry, but not simply by a 90-degree rotation, as would have been predicted if polarity correlated strictly with cell geometry (Figures 3D, 3F, and S4).

Instead, anterior-posterior-directed stretch caused a global and patterned reorganization of Celsr1 polarity, where cells located on either side of the midline reoriented their polarity in opposite directions. This bidirectional shift led to an overall outward rotation of Celsr1 polarity away from the midline, a pattern reminiscent, albeit in reverse, of the polarity shifts observed in the *Drosophila* wing in response to cell flows (Figure S4). Although the degree to which polarity rotated was variable (Figure 3F), the overall pattern of reorientation was reproducible across experiments (Figure S4). The variability we observe is likely due to non-uniform strain across skin explants, which are consistently thicker at the lateral edges and thinnest near the midline. Nevertheless, these results are in stark contrast to controls, which displayed robust and aligned Celsr1 asymmetry across all explants (Figures 3C and 3E). We conclude from these physical manipulations that global tissue deformations can influence the long-range alignment of epidermal PCP.

Interestingly, the loss of strict coupling between Celsr1 localization and cell elongation in this experiment suggested that the axis of polarity is not simply a consequence of cell geometry (Figures 3B and 3D). This notion fits with the observation that whereas, on average, the direction and magnitude of polarity correlates with a gradient of tissue deformation in the embryo, there is poor correlation between polarity and elongation magnitude on a cell-by-cell basis (Figures 2D and S4C). This led us to hypothesize that other mechanisms, such as tension-induced cell rearrangements, may drive the establishment of axial asymmetry.

Oriented Divisions and Cell Rearrangements Accompany Epidermal Deformation

Epithelial cells respond to mechanical strain by undergoing oriented cell divisions and cell rearrangements, which help to relieve overall tissue stress [25]. We reasoned that, because cell divisions and rearrangements require remodeling and de novo formation of intercellular junctions [25], these processes could dramatically alter the distribution of junctionally localized PCP proteins. For example, if Celsr1 homodimers are selectively retained at the persisting junctions through neighbor exchange or division, a strain-induced bias in new junction assembly could orient the axis of Celsr1 asymmetry (Figure 4H) [19]. We therefore monitored division orientations and cell rearrangements as the basal layer transitioned from elongated to relaxed state.

To characterize the effect of tissue strain on epidermal cell behavior, we calculated the planar angles of basal cell divisions in fixed dorsal back skins. At E13.5, basal cells divided in the direction of cell elongation with their telophase spindles oriented within ±30 degrees of the medial-lateral axis (Figures 4A and 4B). Live imaging of E13.5 H2B-GFP embryos further confirmed our data (Figure 4A). The medial-lateral division bias was also observed at E14.5, though to a lesser extent, which is consistent with the more relaxed morphology of basal cells at this stage (Figure 4B). These data fit with the notion that, in response to tissue anisotropy, cells align their division plane with the long axis of the cell. Moreover, the resulting divisions could perhaps facilitate tissue relaxation we observe between E13.5 and E14.5.

We next sought to examine whether basal cells undergo neighbor exchange upon tissue strain. We monitored clones of cells arising from recent divisions and asked whether the two daughters remained in contact or became dispersed. Marked clones were generated by combining the *Brainbow2.1* allele with K14-Cre-ER and injecting low doses of tamoxifen to induce sporadic expression of one of four fluorophores, which allowed unambiguous identification of clonal cell pairs [26, 27]. After 24 hr of induction, most clones consisted of two cells, indicating that they had arisen from a recent division (Figure 4C). When clones were induced at E13.5 and examined at E14.5, daughter cells were frequently separated by at least one cell distance (42% of cell pairs). In contrast, clones induced after tissue relaxation, at E14.5, were separated less frequently (18% of cell pairs) and the majority of daughter cells remained adjoined (Figure 4D). We also observed bridged cell pairs that appeared to be in an intermediate stage of neighbor exchange, in which two daughter cells remained connected by an apical adherens junction but were fully separated by intercalating cells along their basal surface (Figures 4C and 4D). Such intermediates were also observed in z stack images of fixed explants labeled for E-cadherin, where basal cell clusters were arranged into rosette-like structures that formed distinct neighbor connections along apical and basal surfaces (Figure 4E). Importantly, within these "transitional rosettes," it was the medial-lateral interfaces that were predominantly found in an intermediate stage of remodeling (Figure 4G). Moreover, the frequency of rosette-like intermediates was unchanged in PCP mutant (*Vangl2*$^{Lp/Lp}$; Figure 4F), indicating that the process of junctional exchange is not simply a consequence of PCP in the basal layer.

Taken together, our results demonstrate that basal cells undergo oriented cell divisions and extensive neighbor exchanges as the epidermis transitions from an elongated to relaxed morphology and that these neighbor exchanges primarily remodel medial-lateral interfaces. The selective shrinking and expansion of intercellular junctions during cell rearrangements are predicted to have significant consequences on Celsr1 localization (Figure 4H). While oriented divisions also generate new mediolateral interfaces, PCP components internalize into endosomes when basal cells divide [22, 28]. Therefore, we focused specifically on the consequences of neighbor exchange on Celsr1 polarization.

Spontaneous Emergence of Local Celsr1 Polarity In Vitro

Our data indicate that tissue deformation induces junctional rearrangements that selectively affect the dynamics of medial-lateral junctions compared to anterior-posterior junctions. Because long-term live imaging of intact E12–E14 embryos was not feasible, we turned to an in vitro organotypic culture system to address how junctional remodeling impacts Celsr1 asymmetry. Primary keratinocytes were cultured in air-liquid interface (ALI) to induce stratification and differentiation. After ~4 days of growth in ALI, junctional Celsr1 was restricted to the basal layer, mimicking its normal expression pattern in vivo. Within individual basal cells, Celsr1 became asymmetrically distributed, where it preferentially accumulated to some cell interfaces, but not others (Figure 5A). The direction of Celsr1 asymmetry appeared to be locally coordinated between neighboring cells, which we quantified by calculating the average polarity tensors (Mp) within clusters of neighboring cells across several fields of view. Cells and their immediate neighbors displayed significantly higher Mp

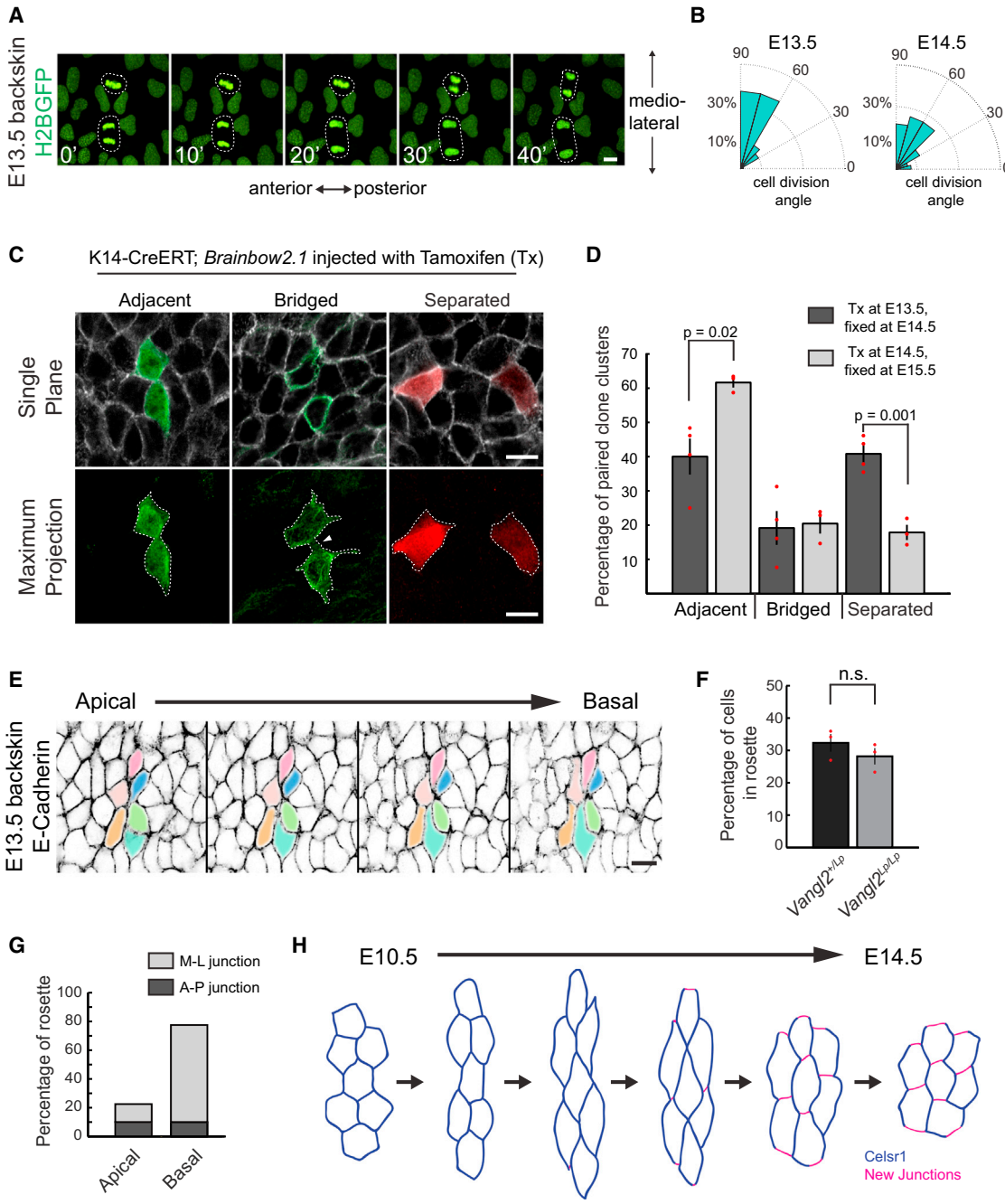

Figure 4. Oriented Divisions and Cell Rearrangements during and after the Establishment of Celsr1 Polarity

(A) Time-lapse images of a K14-H2BGFP transgenic embryo at E13.5. Divisions are oriented along the mediolateral axis.

(B) Quantification of division angles from fixed skin samples, normalized to anterior-posterior axis; E13.5, n = 3 (70 divisions); E14.5, n = 3 (69 divisions).

(C) Induction of clonal cell pairs via recombination of *Brainbow 2.1* reporter activated by low doses of tamoxifen (Tx) injected either at E13.5 or E14.5 and analyzed 24 hours later. Clonal cell pairs are classified as adjacent, bridged, and separated.

(D) Percentage of adjacent, bridged, or separated clones at E14.5 and E15.5 (mean ± SEM); unpaired t test; E14.5, n = 4 (97 clones); E15.5, n = 3 (122 clones).

(E) Confocal images of epithelial cells from the apical to basal surface of E13.5 back skin. Individual cells within a rosette are shaded. Note that adjacent cells at the apical surface are separated basally and vice versa.

(F) Fraction of cells participating in multicellular rosette structures in E14.5 control littermates and *Vangl2*$^{Lp/Lp}$ back skins. Data are represented as mean ± SD (paired t test; n = 3 embryos; 1,698 cells analyzed in control and 2,100 cells analyzed in *Vangl2*$^{Lp/Lp}$).

(G) Analysis of the position and orientation of resolving junctions within multicellular rosettes at E13.5. n = 40 rosettes (from seven embryos).

(H) Model illustrating how directed neighbor exchange, driven by anisotropic cell deformation, could establish and align Celsr1 polarity.

Scale bars represent 10 μm.

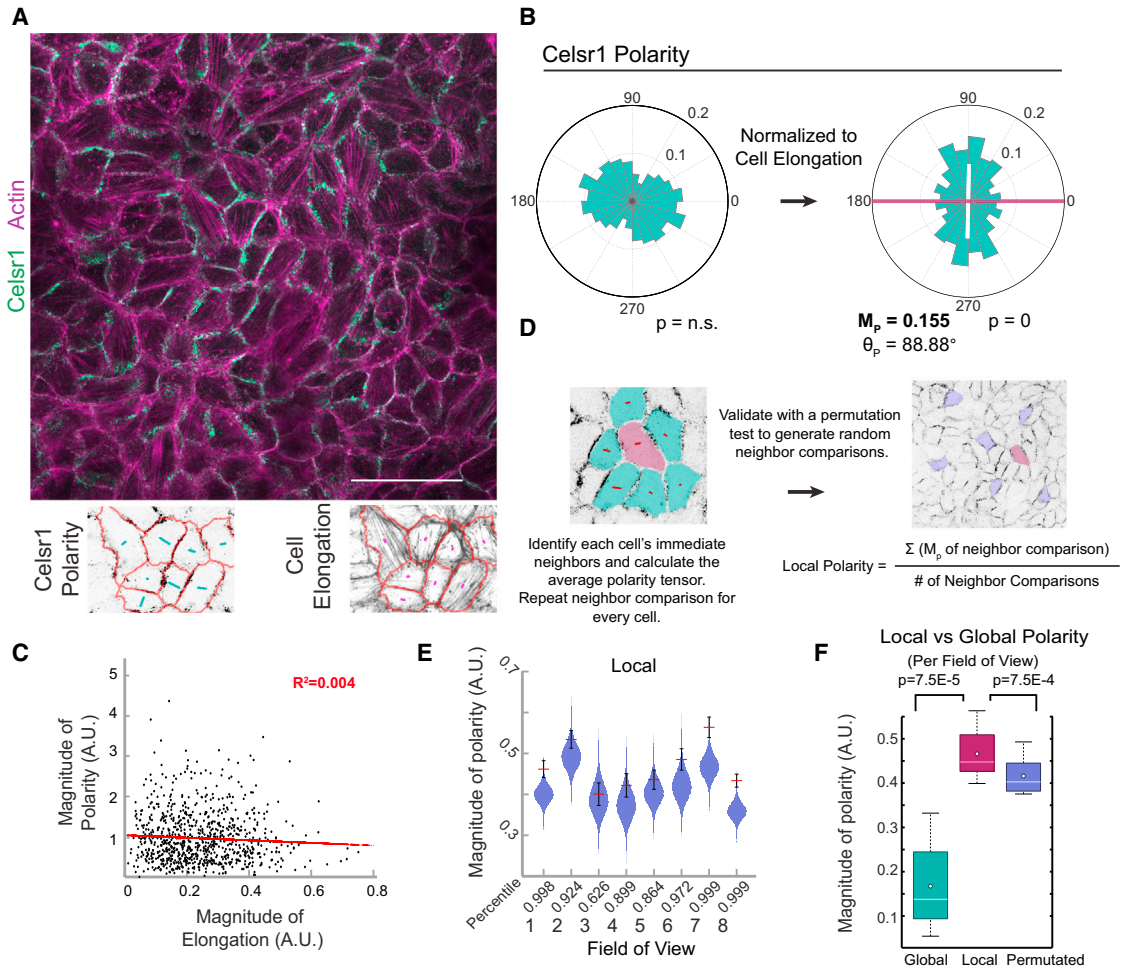

Figure 5. Spontaneous Emergence of Local Polarity In Vitro

(A) Single confocal section of a representative ALI culture labeled with Celsr1 (cyan) and phalloidin (magenta). The scale bar represents 50 μm. Local polarity and elongation tensors are shown below.

(B) Angular distributions for Celsr1 polarity in vitro shown with and without normalization. For normalization, we set the elongation angles to 0°/180° (magenta line) and plotted the corresponding Celsr1 polarities (white line). Note that Celsr1 polarity correlates with cell elongation in vitro. n = 1,919 cells.

(C) Lack of correlation between the magnitudes of Celsr1 polarity and elongation on a cell-by-cell basis.

(D) Schematic for calculation of local polarity. Polarity tensors for each cell are averaged with those from adjacent cells. Local polarity is represented by the mean magnitude all neighbor comparisons (M_p local). Permutation tests were performed to determine the percentile of calculated real-neighbor M_p local with that of 100,000 random comparisons of the same cells.

(E) Violin plots showing the distribution of permutated neighbor comparisons per field of view. M_p local from corresponding real-neighbor comparisons is overlaid (red line; SEM in black).

(F) Global M_p per field of view is compared to corresponding local M_p and average M_p of permutated cells.

p values are determined based on comparisons between collective means (white dots); n = 8 fields of view; 1,919 cells.

values compared to the Mp across the epithelium or to randomly permutated, non-neighboring cells, indicating that planar polarity in vitro is locally coordinated between neighboring cells but randomly oriented across the culture (Figure 5; see figure legend for details). To assess whether the polarity axis was related to local tension, we correlated the orientation of Celsr1 polarity with axes of cell elongation by normalizing the angle of Celsr1 polarity to cell elongation of each cell. When cell elongation angles were set to 0°, Celsr1 polarity was oriented roughly perpendicular, with a mean polarity angle of 88° (Figure 5B), indicating that, on average, Celsr1 asymmetry orients perpendicular to cell elongation in vitro, similar to in vivo. Moreover, the magnitude of polarity correlated poorly with the magnitude of cell elongation on a per cell basis (Figures 5A and 5C). Therefore, in the absence of global cues from the embryo, Celsr1 asymmetry and local alignment emerge spontaneously, providing an in vitro system to monitor the short-range establishment and remodeling of planar polarity.

Local Celsr1 Asymmetry Emerges and Reorganizes upon Neighbor Exchange

To gain further insight into the establishment of Celsr1 polarity in ALI cultures, we performed time-lapse imaging of keratinocytes stably expressing Celsr1-mEos3.2. The basal cells of ALI

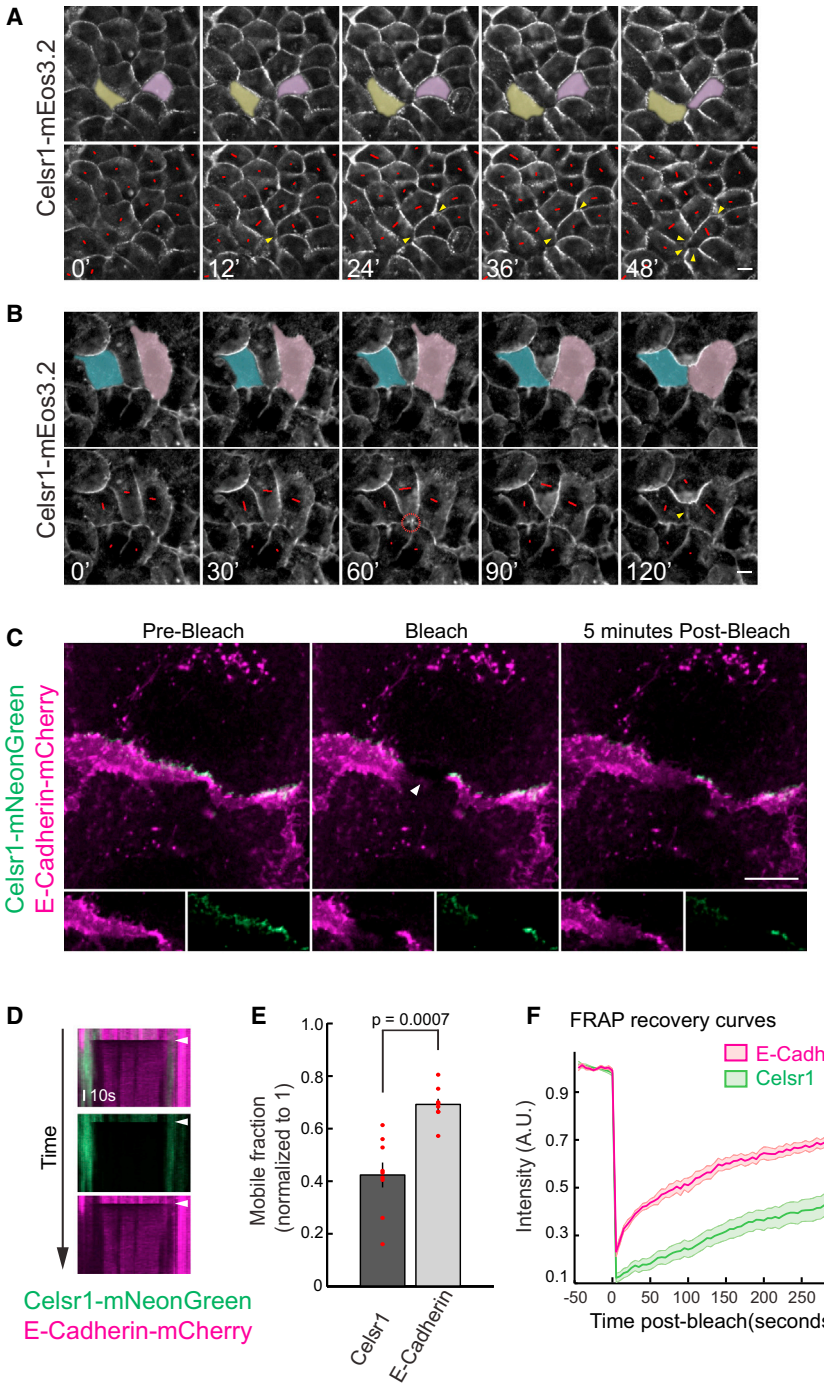

Figure 6. Local Celsr1 Polarity Emerges and Reorients upon Junctional Remodeling

(A) Time-lapse images of a Celsr1-mEos3.2 organotypic culture. Red lines show nematics of Celsr1 polarity. Note that starting from a mostly uniform distribution of Celsr1, Celsr1 polarity emerges as cell forms new junctions (arrowhead) with neighboring cells.

(B) Time-lapse imaging of Celsr1-mEos3.2 organotypic culture shows a rearrangement of Celsr1 polarity upon new junction formation. The red circle highlights the vertex where five cells converge into a point. Arrowhead highlights the new junction.

(C) Representative images of FRAP on Celsr1-mNeonGreen and E-cadherin-mCherry junctions. The arrowhead highlights bleached regions. The bleached region is magnified below.

(D) Kymograph of Celsr1 and E-cadherin recovery after photobleaching. Images are magnified for clarity.

(E) Mobile fraction plots comparing Celsr1 and E-cadherin at junctions (unpaired t test; n = 9 cells).

(F) FRAP curve of Celsr1 (magenta) and E-cadherin (green).

Scale bars represent 10 μm. See also Movies S1, S2, and S3.

cultures were highly dynamic, undergoing numerous cell divisions and neighbor exchanges. During the first few days of culture, basal cells exhibited no detectable Celsr1- mEos3.2 asymmetry. We found that, when cells exchanged neighbors, Celsr1 polarity began to emerge, which was concomitant with the formation of new intercellular junctions. As illustrated in Figure 6A (highlighted cells), Celsr1-mEos3.2 was slow to accumulate at the newly forming junctions between converging cells (Figure 6A, arrowheads), but at the junctions that persisted throughout the rearrangement, Celsr1-mEos3.2 was retained. The selective retention of Celsr1 at persistent cell junctions established Celsr1 asymmetry within the cell cluster, which oriented perpendicular to the nascent junction (Figure 6A). Notably, in cultures that had established Celsr1 asymmetry, neighbor exchange was sufficient to reorient the local axis of polarity. Figure 6B illustrates one such neighbor exchange where two, initially separate, cells converge to form a new intercellular junction. As the newly forming junction elongates, the persistent junctions rotate outward from their common vertex, leading to a shift in the axis of Celsr1 polarity. Thus, in a spontaneously polarizing system, the axis of Celsr1 polarity reflects the position and orientation of persistent junctions.

The observation that Celsr1 polarity can be established through neighbor exchanges implies that turnover of Celsr1 homodimers must be relatively slow, as rapid diffusion or transport into new junctional interfaces would quickly eliminate asymmetry. To assess the relative mobility of Celsr1 at intercellular junctions, we compared fluorescence recovery after photobleaching (FRAP) of E-cadherin and Celsr1 within the same junctions (Figures 6C–6F). FRAP measurements were performed on cell-cell contacts between keratinocytes co-expressing E-cadherin-mCherry and Celsr1-mNeonGreen. Indeed, Celsr1-mNeonGreen recovered much more slowly than E-cadherin-mCherry (Figures 6D–6F). Moreover, when compared with E-cadherin, the average mobile

fraction of Celsr1 was significantly lower (Figures 6E and 6F; average mobile fraction 42.3% ± 4.8% versus 69% ± 2.1%), demonstrating a lower turnover rate for Celsr1 junctions. The difference in dynamics between E-cadherin and Celsr1 could explain why junctional remodeling is sufficient to polarize Celsr1, but not E-Cadherin, localization.

DISCUSSION

The skin is a remarkable example of long-range PCP where polarity collectively aligns across the entire body surface. To generate this pattern, global cues must instruct both the polarity vector, to bias Fz and Vangl complexes to opposite poles of the cell, as well as the polarity axis, to restrict PCP complex localization along a single plane. Here, we demonstrate that, during the initiation of PCP asymmetry, a gradient of tissue deformation forms along the medial-lateral axis of the dorsal epidermis, which possibly serves as a global cue that distinguishes two planar axes of the tissue. As a wave of cell deformations extends laterally from the dorsal midline, Celsr1 asymmetry matures asynchronously along the medial-lateral axis. Initially, the magnitude and direction of polarity are tightly linked to the degree and orientation of tissue elongation. Later, maximal Celsr1 asymmetry is achieved as the tissue relaxes to a more isotropic state. The source of tissue deformation in the skin is currently unknown, but one possibility is that anisotropic growth of the embryo exerts uniaxial strain exogenously on the overlying epidermis. Alternatively, dermal alignment and epithelial elongation may represent inherent elements of embryonic skin patterning. Indeed, medial-lateral cell elongation coupled with rearrangement of intercellular junctions invokes a process reminiscent of convergent extension.

Several observations link the polarity axis to junctional rearrangements. The anisotropic cell shapes we observe indicate the presence of mechanical stress within the tissue. To relieve tissue stress, epithelial cells are known to undergo neighbor exchange [25], which requires removal of existing cell-cell contacts and formation of new cell-cell boundaries. Because the interfaces that persist during cell rearrangements selectively retain PCP complexes, dynamic junctional changes can have profound effects on the axis of PCP asymmetry, as previously shown in the *Drosophila* wing [19]. We find that basal cells also actively remodel intercellular junctions, as evidenced by the presence of dispersed clones and epithelial rosettes throughout the embryonic epidermis. We propose that medial-lateral-directed tissue deformation biases the orientation of junctional dynamics in the basal layer, such that anterior-posterior interfaces selectively persist through cell rearrangements. Given the relative immobility of junctionally localized Celsr1, and the fact that Celsr1 homodimers cannot cross into a new junctional interface without first dissociating and diffusing as a monomer, a mechanism where new junction formation is directionally biased is predicted to establish robust and coordinated PCP domains along a single tissue axis (Figure 4G).

Combined with the yet unknown vectorial cues that bias Fz and Vangl complexes to opposite poles, the observed mechanical strain and geometric changes in the mouse epidermis may facilitate and enhance the feedback interactions that underlie vectorial asymmetry. Unlike hexagonally packed epithelia, the basal layer of skin is comprised of mixed polygons where cell junctions do not neatly align along the tissue axes. These irregular epithelial geometries present a challenge for effective feedback propagation of polarity across the epithelium. This has been observed experimentally in the *Drosophila* wing, where disruptions to PCP most commonly occur at wing veins where cell shapes deviate from the typical hexagonal array [29]. In skin, collective cell elongation transforms poorly aligned junctions into parallel arrays that are coordinated with the body axes. The generation and alignment of cell edges depleted for Celsr1 junctions establishes a global axis orthogonal to Fz and Vang vectors in which feedback interactions cannot take place, thereby strengthening the intercellular coordination of PCP.

Mechanical forces have been shown to coordinate global planar polarity in other contexts, indicating that tissue deformation can function as a versatile yet fundamental mechanism for setting up and refining the PCP axis [19, 30, 31]. In the *Drosophila* wing imaginal disc, morphogenetic gradients promote polarized tissue growth, which has been proposed to orient the initial PCP pattern [31]. Later, during pupal wing morphogenesis, anisotropic tissue tension causes cell flow and a global reorientation of PCP across tissue [19]. Moreover, the first signs of PCP asymmetry in *Xenopus* coincide with the gastrulation movements that drive early embryo elongation [32]. Our data demonstrate that the murine epidermis undergoes similar, global morphogenetic changes that establish and coordinate Celsr1 asymmetry across the mammalian skin, suggesting that mechanical induction of PCP alignment is a conserved and fundamental feature of PCP from flies to mammals.

EXPERIMENTAL PROCEDURES

Experimental procedures include immunostaining, explant culture, cell culture, imaging, FRAP, and image analysis. All procedures involving animals were in accordance with the Guide for the Care and Use of Laboratory Animals and approved by Princeton University's Institutional Animal Care and Use Committee (IACUC). Full details can be found in the Supplemental Experimental Procedures.

SUPPLEMENTAL INFORMATION

Supplemental Information includes Supplemental Experimental Procedures, four figures, and three movies and can be found with this article online at http://dx.doi.org/10.1016/j.cub.2016.06.030.

AUTHOR CONTRIBUTIONS

W.Y.A. performed in vivo experiments and analyzed the data. B.W.H. contributed to data analysis and performed organotypic culture experiments. B.J. designed and performed the clonal inductions. D.D. oversaw the experimental design and analysis and wrote the manuscript.

ACKNOWLEDGMENTS

We kindly thank Benoit Aiguoy for providing Packing Analyzer. We thank Gary Laevsky and the Nikon Center of Excellence for generous assistance with imaging and Katherine Little for purifying the Celsr1 antibody and general lab assistance. We are grateful to Eric Wieschaus, Jean Schwarzbauer, Jared Toettcher, Rachel Kadzik, and D.D. lab members for helpful discussions and comments on the manuscript. This work was supported by NIH/NIAMS grant R01AR066070 as well as the Searle Scholars Program and the Vallee

Foundation. W.Y.A. holds an American Heart Association predoctoral fellowship, and B.W.H. is supported by an NSF-GRFP Award.

Received: January 7, 2016
Revised: May 16, 2016
Accepted: June 15, 2016
Published: July 21, 2016

REFERENCES

1. Goodrich, L.V., and Strutt, D. (2011). Principles of planar polarity in animal development. Development *138*, 1877–1892.
2. Vladar, E.K., Antic, D., and Axelrod, J.D. (2009). Planar cell polarity signaling: the developing cell's compass. Cold Spring Harb. Perspect. Biol. *1*, a002964.
3. Simons, M., and Mlodzik, M. (2008). Planar cell polarity signaling: from fly development to human disease. Annu. Rev. Genet. *42*, 517–540.
4. Devenport, D. (2014). The cell biology of planar cell polarity. J. Cell Biol. *207*, 171–179.
5. Shimada, Y., Usui, T., Yanagawa, S., Takeichi, M., and Uemura, T. (2001). Asymmetric colocalization of Flamingo, a seven-pass transmembrane cadherin, and Dishevelled in planar cell polarization. Curr. Biol. *11*, 859–863.
6. Usui, T., Shima, Y., Shimada, Y., Hirano, S., Burgess, R.W., Schwarz, T.L., Takeichi, M., and Uemura, T. (1999). Flamingo, a seven-pass transmembrane cadherin, regulates planar cell polarity under the control of Frizzled. Cell *98*, 585–595.
7. Strutt, H., and Strutt, D. (2008). Differential stability of flamingo protein complexes underlies the establishment of planar polarity. Curr. Biol. *18*, 1555–1564.
8. Devenport, D., and Fuchs, E. (2008). Planar polarization in embryonic epidermis orchestrates global asymmetric morphogenesis of hair follicles. Nat. Cell Biol. *10*, 1257–1268.
9. Bastock, R., Strutt, H., and Strutt, D. (2003). Strabismus is asymmetrically localised and binds to Prickle and Dishevelled during Drosophila planar polarity patterning. Development *130*, 3007–3014.
10. Strutt, D.I. (2001). Asymmetric localization of frizzled and the establishment of cell polarity in the Drosophila wing. Mol. Cell *7*, 367–375.
11. Strutt, D. (2009). Gradients and the specification of planar polarity in the insect cuticle. Cold Spring Harb. Perspect. Biol. *1*, a000489.
12. Harumoto, T., Ito, M., Shimada, Y., Kobayashi, T.J., Ueda, H.R., Lu, B., and Uemura, T. (2010). Atypical cadherins Dachsous and Fat control dynamics of noncentrosomal microtubules in planar cell polarity. Dev. Cell *19*, 389–401.
13. Shimada, Y., Yonemura, S., Ohkura, H., Strutt, D., and Uemura, T. (2006). Polarized transport of Frizzled along the planar microtubule arrays in Drosophila wing epithelium. Dev. Cell *10*, 209–222.
14. Matis, M., Russler-Germain, D.A., Hu, Q., Tomlin, C.J., and Axelrod, J.D. (2014). Microtubules provide directional information for core PCP function. eLife *3*, e02893.
15. Klein, T.J., and Mlodzik, M. (2005). Planar cell polarization: an emerging model points in the right direction. Annu. Rev. Cell Dev. Biol. *21*, 155–176.
16. Adler, P.N., Krasnow, R.E., and Liu, J. (1997). Tissue polarity points from cells that have higher Frizzled levels towards cells that have lower Frizzled levels. Curr. Biol. *7*, 940–949.
17. Lawrence, P.A., Casal, J., and Struhl, G. (2004). Cell interactions and planar polarity in the abdominal epidermis of Drosophila. Development *131*, 4651–4664.
18. Le Garrec, J.F., Lopez, P., and Kerszberg, M. (2006). Establishment and maintenance of planar epithelial cell polarity by asymmetric cadherin bridges: a computer model. Dev. Dyn. *235*, 235–246.
19. Aigouy, B., Farhadifar, R., Staple, D.B., Sagner, A., Röper, J.C., Jülicher, F., and Eaton, S. (2010). Cell flow reorients the axis of planar polarity in the wing epithelium of Drosophila. Cell *142*, 773–786.
20. Guo, N., Hawkins, C., and Nathans, J. (2004). Frizzled6 controls hair patterning in mice. Proc. Natl. Acad. Sci. USA *101*, 9277–9281.
21. Ravni, A., Qu, Y., Goffinet, A.M., and Tissir, F. (2009). Planar cell polarity cadherin Celsr1 regulates skin hair patterning in the mouse. J. Invest. Dermatol. *129*, 2507–2509.
22. Devenport, D., Oristian, D., Heller, E., and Fuchs, E. (2011). Mitotic internalization of planar cell polarity proteins preserves tissue polarity. Nat. Cell Biol. *13*, 893–902.
23. Butler, M.T., and Wallingford, J.B. (2015). Control of vertebrate core planar cell polarity protein localization and dynamics by Prickle 2. Development *142*, 3429–3439.
24. Vladar, E.K., Bayly, R.D., Sangoram, A.M., Scott, M.P., and Axelrod, J.D. (2012). Microtubules enable the planar cell polarity of airway cilia. Curr. Biol. *22*, 2203–2212.
25. Guillot, C., and Lecuit, T. (2013). Mechanics of epithelial tissue homeostasis and morphogenesis. Science *340*, 1185–1189.
26. Snippert, H.J., van der Flier, L.G., Sato, T., van Es, J.H., van den Born, M., Kroon-Veenboer, C., Barker, N., Klein, A.M., van Rheenen, J., Simons, B.D., and Clevers, H. (2010). Intestinal crypt homeostasis results from neutral competition between symmetrically dividing Lgr5 stem cells. Cell *143*, 134–144.
27. Vasioukhin, V., Degenstein, L., Wise, B., and Fuchs, E. (1999). The magical touch: genome targeting in epidermal stem cells induced by tamoxifen application to mouse skin. Proc. Natl. Acad. Sci. USA *96*, 8551–8556.
28. Shrestha, R., Little, K.A., Tamayo, J.V., Li, W., Perlman, D.H., and Devenport, D. (2015). Mitotic control of planar cell polarity by polo-like kinase 1. Dev. Cell *33*, 522–534.
29. Ma, D., Amonlirdviman, K., Raffard, R.L., Abate, A., Tomlin, C.J., and Axelrod, J.D. (2008). Cell packing influences planar cell polarity signaling. Proc. Natl. Acad. Sci. USA *105*, 18800–18805.
30. Olguín, P., Glavic, A., and Mlodzik, M. (2011). Intertissue mechanical stress affects Frizzled-mediated planar cell polarity in the Drosophila notum epidermis. Curr. Biol. *21*, 236–242.
31. Sagner, A., Merkel, M., Aigouy, B., Gaebel, J., Brankatschk, M., Jülicher, F., and Eaton, S. (2012). Establishment of global patterns of planar polarity during growth of the Drosophila wing epithelium. Curr. Biol. *22*, 1296–1301.
32. Chien, Y.H., Keller, R., Kintner, C., and Shook, D.R. (2015). Mechanical strain determines the axis of planar polarity in ciliated epithelia. Curr. Biol. *25*, 2774–2784.